



Published in final edited form as:

J Aerosol Sci. 2010 March 1; 41(3): 257–265. doi:10.1016/j.jaerosci.2010.01.003.

GAS-PHASE FLAME SYNTHESIS AND PROPERTIES OF MAGNETIC IRON OXIDE NANOPARTICLES WITH REDUCED OXIDATION STATE

Benjamin M Kumfer^{a,1}, Kozo Shinoda^b, Balachandran Jeyadevan^c, and Ian M Kennedy^a

^aDepartment of Mechanical and Aeronautical Engineering, University of California Davis, CA 95616 USA

^bInstitute of Multidisciplinary Research for Advanced Materials, Tohoku University, Sendai, 980-8577, Japan

^cGraduate School of Environmental Studies, Tohoku University, Sendai 980-8579, Japan

Abstract

Iron oxide nanoparticles of reduced oxidation state, mainly in the form of magnetite, have been synthesized utilizing a new continuous, gas-phase, nonpremixed flame method using hydrocarbon fuels. This method takes advantage of the characteristics of the inverse flame, which is produced by injection of oxidizer into a surrounding flow of fuel. Unlike traditional flame methods, this configuration allows for the iron particle formation to be maintained in a more reducing environment. The effects of flame temperature, oxygen-enrichment and fuel dilution (i.e. the stoichiometric mixture fraction), and fuel composition on particle size, Fe oxidation state, and magnetic properties are evaluated and discussed. The crystallite size, Fe(II) fraction, and saturation magnetization were all found to increase with flame temperature. Flames of methane and ethylene were used, and the use of ethylene resulted in particles containing metallic Fe(0), in addition to magnetite, while no Fe(0) was present in samples synthesized using methane.

Keywords

magnetite; superparamagnetic; flame synthesis; nanoparticles; iron oxide

1. Introduction

Gas-phase flame synthesis is an attractive method for the synthesis of nanoscale metal oxides because of the great potential for large-scale production (Pratsinis 1998; Wooldridge 1998), as evidenced by the production of fumed silica, titania, and zinc oxides at rates approaching millions of tons/year (Stark and Pratsinis 2002). While metal oxides have been synthesized using a number of flame configurations, a straightforward and readily scalable method utilizes

© 2010 Elsevier Ltd. All rights reserved.

address correspondence to: Ian M. Kennedy, University of California, Dept. Mechanical and Aeronautical Engineering, One Shields Ave., Davis, CA 95616, Ph: (530) 752-2796, Fax: (530) 752-4158, imkenney@ucdavis.edu.

¹present address: Department of Energy, Environmental and Chemical Engineering, Washington University, St. Louis, MO 63130

Publisher's Disclaimer: This is a PDF file of an unedited manuscript that has been accepted for publication. As a service to our customers we are providing this early version of the manuscript. The manuscript will undergo copyediting, typesetting, and review of the resulting proof before it is published in its final citable form. Please note that during the production process errors may be discovered which could affect the content, and all legal disclaimers that apply to the journal pertain.

a non-premixed jet flame, which is formed from the injection of a gaseous fuel (hydrogen or a hydrocarbon) into a surrounding flow of oxidizer (air or oxygen-enriched air). In this flame configuration, there is an abundance of oxygen at high temperature available for oxidation of the metal: the excess oxidant makes it difficult to control the final oxidation state of the product. For example, the introduction of iron pentacarbonyl into a hydrogen/air diffusion flame has been found to result in only fully oxidized Fe(III), largely in the form of maghemite (γ -Fe₂O₃) (Guo and Kennedy 2007). Upon inspection of the phase diagram for the Fe-O system, it is evident that the synthesis of reduced iron oxides, such as Fe₃O₄ or FeO, would not be thermodynamically favorable in a typical flame configuration because the oxygen concentration in the region of particle formation is too large. There is widespread interest in nanoscale Fe₃O₄ (magnetite) because of its catalytic and magnetic properties for applications in magnetic recording and sensing, magnetic fluids, magnetic resonance imaging, and biosensors. A scalable aerosol route for the production of these materials would be very useful.

An *inverse* diffusion flame offers an attractive alternative for the synthesis of nanoparticles of transition metal oxides. An inverse diffusion flame is created by the injection of oxidizer into a surrounding flow of fuel. This flame provides a unique environment for nanoparticle formation. The inverse flame configuration has been previously utilized in the synthesis of metal oxide nanoparticles, resulting in drastically different particle morphology and crystallinity than those made by classic diffusion flames (Pratsinis *et al.* 1996; Zhu and Pratsinis 1997). Studies of soot in laminar inverse flames have shown that soot particles form on the fuel-side of the stoichiometric flame location and are transported away from the flame as a consequence of the flow field and thermophoresis – particles do not cross the stoichiometric location or pass into the oxidizer-side, and are isolated in a fuel-rich environment (Makel and Kennedy 1994; Sidebotham and Glassman 1992; Wu and Essenhigh 1986). Unrau *et al.* (2007) utilized this characteristic of the inverse flame for the aerosol synthesis of carbon nanotubes. Similarly, by introducing a metal precursor with the fuel, nanoparticles may be synthesized in a fuel-rich, reduced-oxygen environment, offering the potential for producing transition metal oxides with a reduced oxidation state. Other studies using flame spray systems have demonstrated that by maintaining a reducing atmosphere, reduced metal oxides or even pure metals can be synthesized (Grass and Stark 2006a; b). Our focus is the magnetic iron oxide, magnetite (Fe₃O₄).

Flame methods have been successfully applied in the synthesis of Fe₂O₃ (Grimm *et al.* 1997; Janzen and Roth 2001; Li *et al.* 2007; Zachariah *et al.* 1995), but application to the synthesis of Fe₃O₄ has been far more limited. Popular methods for the synthesis of magnetite include a variety of solution/precipitation techniques that are not well-suited for large-scale production. Several aerosol synthesis methods for magnetite have been developed which involve the thermal decomposition of iron precursors in a furnace (Cabanas *et al.* 1993; Langlet *et al.* 1986; Schleicher *et al.* 1998; Tang *et al.* 1989). However, production rates via these methods are limited. Gonzalez *et al.* (2007) employed an electrospray to synthesize carbon-coated magnetite. Mixtures of α -Fe, γ -Fe₂O₃ and Fe₃O₄ particles have been produced using flame spray pyrolysis (Makela *et al.* 2004) and laser-induced pyrolysis (Hofmeister *et al.* 2001) methods. Other reported methods for Fe₃O₄ that utilize a flame include the so-called “flame fusion” method (Miyake *et al.* 1999), which involves the injection of iron powders into a high temperature flame in which they become oxidized and spherical, and a gas-phase method that makes use of the decomposition of Fe(CO)₅ in a bunsen-type flame (Urakawa *et al.* 1996).

We report the synthesis of reduced iron oxide nanoparticles in a laminar inverse diffusion flame. While the particle production rate that can be achieved in a laminar flame is very limited in comparison to that of turbulent flames, we choose the laminar flame for this study to extract fundamental information without potential complications arising from turbulent mixing

effects. The effects of flame temperature, flame structure, and fuel composition on the particle size, Fe speciation, and magnetic properties are investigated.

2. Experiment

A laminar, inverse diffusion flame was stabilized on a burner that provided three concentric gas flows. A schematic of the burner and particle collection system is provided in Fig. 1. This burner was similar in construction to that described by Kumfer et al. (2008). It consisted of two concentric brass tubes, with outer diameters of 0.95 cm and 1.9 cm, enclosed within a chamber made of acrylic tubing with an inner diameter of 11.4 cm. The enclosure is critical in order to isolate the flame from room air, thereby preventing further oxidation of particles downstream of the flame and preventing the formation of a secondary diffusion flame front that may form due to reaction of excess fuel with room air. Oxidizer (either 100% O₂ or O₂ diluted with argon) exited the inner-most tube. The flow of oxidizer was surrounded by a mixture containing fuel (either methane or ethylene), argon, and the iron precursor vapor. The total amount of fuel supplied was in large excess of that required for stoichiometric consumption of the oxygen, resulting in an overall fuel-rich system. The resulting inverse flame was surrounded by a flow of N₂. Iron pentacarbonyl (Alfa Aesar, 99.5%), Fe(CO)₅, was the chosen precursor. Argon was bubbled through liquid Fe(CO)₅. The Fe(CO)₅ bubbler was kept in an ice bath to maintain a constant vapor pressure. The flow rate of argon through the bubbler was held constant, thus the delivery rate of Fe(CO)₅ was also fixed. Assuming that the mixture leaving the bubbler was saturated, the delivery rate of Fe(CO)₅ was 57 mg/hr. The fuel/argon/Fe(CO)₅ mixture flow rate was maintained at 1.2 LPM. The oxidizer flow rate was varied to maintain a constant flame height of 30 mm throughout these experiments. This was done in attempt to maintain constant particle residence time in the high temperature zone, which may be characterized by the flame height divided by the gas velocity. The flame exhaust containing the iron oxide aerosol was passed through a diffusion dryer (TSI Inc.) to remove moisture. Particles were collected on a PTFE membrane filter with a pore size of 0.2 μm (Advantec Inc.).

Iron oxide particles were sampled thermophoretically from the flame at a height of approximately 20 mm from the visible flame tip, and deposited onto TEM grids using the rapid insertion technique described by Dobbins and Megaridis (1987). The sampling probe was injected through a port in the chamber wall. Particle size and morphology were determined using a Phillips CM-12 transmission electron microscope. Magnetic properties were measured at room temperature using a vibrating sample magnetometer (VSM). The crystal structure of iron oxide particles was analyzed using a Rigaku RINT2200 X-ray diffractometer with a Cu-Kα radiation source. The short range structure of iron oxide was determined by X-ray absorption spectroscopy (XAS) using a Rigaku R-XAS X-ray spectrometer (Taguchi *et al.* 2005) operating in transmission mode. A Si(400) Johansson-type bent single crystal was used for the monochromator. Samples were mixed with BN powder and pelletized.

The majority of the flames in this study were created by injecting pure O₂ into diluted fuel. Hence, the stoichiometric mixture fraction, Z_{st} , is significantly greater than that of a typical pure fuel/air flame. The stoichiometric mixture fraction is the mass fraction of species that originated from the fuel stream, at the location of stoichiometry, and is defined as

$$Z_{st} = (1 + Y_{F,0} W_O \nu_O / Y_{O,0} W_F \nu_F)^{-1}, \quad (1)$$

where $Y_{F,0}$ and $Y_{O,0}$ denote the fuel and oxidizer mass fractions at the inlet, W_F and W_O are the fuel and oxidizer species molecular weights, and ν_F and ν_O are the fuel and oxygen stoichiometric coefficients, respectively. Soot formation in diffusion flames is drastically reduced upon the increase of Z_{st} (Du and Axelbaum 1995; Kumfer *et al.* 2008; Kumfer *et al.*

2006; Sunderland *et al.* 2004). Measurements of the sooting limits in both inverse and normal co-flow flames have demonstrated that the flame temperature which results in the onset of soot formation increases dramatically with Z_{st} (Kumfer *et al.* 2008; Kumfer *et al.* 2006). For this reason, the high- Z_{st} flame is advantageous for nanoparticle synthesis in hydrocarbon flames since a much higher flame temperature can be attained before soot contamination becomes problematic. In the absence of $Fe(CO)_5$, all of the flames in this study appeared completely blue and no yellow/orange luminosity could be observed from soot particles in a completely dark room. In addition, filter samples were collected in the absence of Fe precursor, and no particles were observed on the filter. Nonetheless, the presence of some carbon within the iron particles cannot be completely ruled out. Another advantage of the high- Z_{st} flame is that it is less susceptible to lift-off or blow-out than are flames of lower Z_{st} , in the inverse configuration (Kumfer 2005).

3. Results

Particle samples from five different flames (denoted A thru E) were collected for analysis. For each flame, the adiabatic flame temperature, T_{ad} , was calculated using the CEA equilibrium code (McBride and Gordon 1996), although this is an overestimate of the actual flame temperature. The adiabatic temperature, fuel and oxidizer boundary mole fractions, and the stoichiometric mixture fraction for each flame are summarized in Table 1. The effects of flame temperature on the particle properties can be best observed by comparing results from flames B, C and D, which are all methane flames of high Z_{st} . The effects of varying Z_{st} can be best observed by comparing samples A and B, which exhibit very similar flame temperatures. Lastly, the effects of replacing methane with ethylene can be observed by comparing C and E, which are of equal T_{ad} and Z_{st} .

X-ray diffraction patterns of several iron oxide particle samples are shown in Fig. 2. The spinel structure is the only structure identified from the XRD patterns of samples A – D. The spinel structural feature in sample A appears to be represented even though the diffraction peak width is very large. The spinel structure is characteristic of both magnetite and maghemite, thus it is very difficult to distinguish between these two possible iron oxide species based on XRD. In sample E, an additional peak at approximately 45 degrees is present, which corresponds to the main diffraction peak of cubic iron metal (α -Fe). The particles were not kept in an inert environment. In view of the high reactivity of nanoscale Fe(0) with oxygen, it is hypothesized that the Fe metal phase is contained within a protective shell of a spinel structured iron oxide. The oxide crystallite diameter, D_{cr} , was calculated from Scherrer's formula applied to the peak at 35 degrees. These results are listed in Table 1. The crystallite diameter is found to increase with flame temperature.

Particles were thermophoretically sampled from each flame and analyzed by TEM. Amongst all of the experiments, flame A yielded the smallest particle size and flame D yielded the largest, and images of particles from these two samples are shown in Fig. 3. The particles are aggregates composed of smaller primary particles. The unusually long and straight chains observed in sample A are quite unique in comparison to other flame-generated materials. This preferentially linear chain morphology has also been observed in iron particles contained in welding fumes (Zimmer and Biswas 2001) and is caused by the alignment of magnetic dipoles (Kumar and Biswas 2005).

X-ray absorption spectra of the near-edge structure (XANES) region at Fe K absorption edge were measured and compared with the spectra of reference Fe foil, Fe_3O_4 and various Fe(III) standard reference materials (RARE METALLIC Co., Ltd.). Backgrounds in the measured absorbance spectra were estimated by extrapolation of the spline function fitted to pre-edge absorbance. After the background was subtracted, the spectra were normalized by using

absorbance calculated under the assumption of isolated Fe atom. Measurements of the XANES spectra can be utilized to distinguish between magnetite and fully oxidized iron oxide by observing the relative energy positions of the absorption edges. The XANES spectra from sample A and the reference Fe_3O_4 material are shown together in Fig. 4a. The Fe K absorption edge energy position of sample A is above that of Fe_3O_4 , which is indicative of higher oxidation state (O'Day *et al.* 2004). After comparing the spectrum of sample A with those of the Fe(III) standard materials (not shown) we conclude that sample A is nearly entirely composed of Fe (III). For samples A, C and D, the measured energy positions of the absorption edge were 1.2 eV, 0.6 eV and 0.4 eV above that for pure magnetite, respectively. With an increase in Z_{st} and flame temperature (comparing samples A and C), the relative edge position decreases, hence the fraction of Fe(II) increases. This is also evidenced by the color of the particles, which transitions from a dark brown to black with increasing Fe(II). In considering the XAFS, XRD, and TEM results together, we conclude that sample C is composed of a mixture of sample A and magnetite. The XANES profile of sample C can be represented by summation of weighted XANES spectra of sample A and magnetite, and the best fit was obtained for 0.65 sample A + 0.35 magnetite. By comparing the relative edge positions of samples C and D (0.6 and 0.4 eV, respectively), the effect of flame temperature on oxidation state is isolated. Increasing the adiabatic flame temperature to 2650 K results in a fraction of Fe(II) that approaches that of pure magnetite (for Fe_3O_4 , the ratio of Fe(II) to Fe(III) is 1:2).

The XANES analysis of sample E provides further evidence of the presence of Fe metal in this sample. The pre-edge peak is high and the edge gradient is weak in comparison to that of the Fe_3O_4 reference material. The XANES spectra of sample E, Fe_3O_4 , and Fe metal foil reference material are shown together in Fig. 4b. The spectrum of sample E was fitted by summation of weighted XANES spectra of Fe metal foil and sample C, and the best fit was obtained for 0.14 Fe + 0.86 sample C.

The saturation magnetization, M_s , and the coercivity, H_c , obtained from the VSM measurements are listed in Table 1. Sample E exhibited the largest M_s , due largely to the addition of α -Fe, which has a larger M_s than that of magnetite. The sample with the lowest M_s is sample A, which also has the smallest crystallite diameter and largest fraction of Fe(III). Hysteresis curves from samples B, C and D are plotted in Fig. 5. The saturation magnetization is found to increase with flame temperature. This trend may be attributed to crystallite size effects. The M_s for bulk magnetite is reported to be 92 emu/g (du Trémolet de Lacheisserie *et al.* 2005); however, below a critical grain size, M_s is known to decrease with decreasing size (Hergt *et al.* 1998). In addition, considering that the XANES spectra of samples, C and D could be represented by a mixture of sample A (which has a low M_s), and magnetite, the trend could be explained by an increase in the fraction of magnetite with flame temperature.

The bulk material has a very small coercivity, indicating that the majority of the particles are exhibiting superparamagnetic behavior. This is not surprising since, for every sample measured, the mean crystallite size measured by XRD is less than the critical grain size for the transition to superparamagnetic behavior, which occurs at around 20 nm (Hergt *et al.* 1998). As can be seen from the TEM images, there is a size distribution of primary particles. The measured coercivity can therefore be attributed to those relatively few particles in the bulk sample that are larger than the critical size.

4. Discussion

The preceding results reveal that the stoichiometric mixture fraction, flame temperature, and fuel composition may be varied for the purpose of controlling the particle size, oxidation state, and magnetic properties of iron oxide nanoparticles. In the following, the effects of each of these flame parameters are examined in more detail, beginning with Z_{st} . By changing Z_{st} , the

flame structure, which refers to the species profiles in relation to the temperature profile, is altered. As a consequence of increasing Z_{st} , the local atomic carbon to oxygen ratio (C/O) on the fuel-side of the flame – at a given temperature – is decreased. The relationship between the local temperature, T , and C/O ratio is given in Eq. 2, which was first presented by Sunderland et al. (2004) and derived by employing the classical Burke-Schumann, conserved scalar approach.

$$C/O(T) = \frac{m}{2(m+n/4)} \left[\frac{1}{Z_{st}} \frac{(T_f - T)}{(T - T_0)} + 1 \right] \quad (2)$$

The variables m and n denote the number of carbon and hydrogen atoms respectively in the fuel molecule, C_mH_n . T_f and T_0 are the flame temperature and the boundary temperature (gas temperature at burner exit), respectively.

The C/O ratio has been routinely employed as a measure of the tendency for soot formation and represents the competition for carbon between soot formation and carbon oxidation. The local C/O ratio can also be viewed as an indicator for the reductive or oxidative potential for iron oxides. A large C/O ratio is indication of a fuel-rich environment that is more conducive to forming reduced oxides, while a small C/O ratio is more conducive to oxidation. Consider the local temperature on the fuel side at which $Fe(CO)_5$ decomposes, releasing CO and Fe(0), $T = T_d$ (approx. 325 °C (Smirnov 1993)). As demonstrated by Eq. 2, when the flame temperature is held constant, increasing Z_{st} results in a decrease of the C/O ratio at the location of T_d . Hence, one might expect that this would result in the formation of iron oxide particles having an increased oxidation state. However, comparing the XANES spectra in samples A and C, the opposite trend is observed with the increase in Z_{st} from 0.35 to 0.85. To understand this result, the other consequences of increasing Z_{st} must be considered.

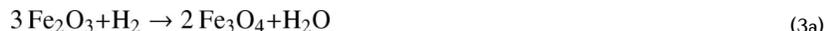
Changing Z_{st} also affects the shape of the flame. For the inverse diffusion flame, an increase of Z_{st} shifts the stoichiometric flame location further into the oxidizer stream, resulting in a taller and wider flame (for constant oxidizer flow rate). In order to maintain constant flame height, the oxidizer flow rate for flame A ($Z_{st} = 0.35$) is higher than that of flame B ($Z_{st} = 0.85$) by more than a factor of four. The increase in jet flow rate leads to steeper temperature gradients and increased convection towards the fuel-side (Kumfer *et al.* 2008). In addition, the flame is curved inwards towards the oxidizer. Hence, particle transport in the direction away from the flame location via convection and thermophoresis is increased in flame A. On the other hand, in the high- Z_{st} flame, the flame is curved outward into the fuel stream, and the temperature gradients are weaker. As a result, particles may penetrate further towards the flame, entering a region of higher temperature. In fact, this was indicated by the appearance of the flames in this study: in flames B, C, D & E, an orange-yellow luminous region on the fuel-side of the flame was observed due to iron oxide particles at high temperature while no such luminosity was observed in flame A. This evidence suggests that the Fe(III) material synthesized in flame A is a unique and undesirable result of particle formation and growth occurring very far away from the stoichiometric flame location and at a relatively low temperature. The oxidation of Fe(0) released from the decomposition of $Fe(CO)_5$ is likely due to low temperature reaction with flame products, and not to reactions with intermediate oxygen-containing species in the high-temperature flame zone.

The XRD and TEM analysis of samples B, C and D show that increasing the flame temperature leads to larger particles with a larger crystallite size, as expected since the rates of particle collision, sintering, and crystal growth are all known to increase with temperature. In addition, the XANES spectra reveal that the fraction of Fe(II) also increases with flame temperature. In the case of flames B, C and D, changes in flame shape and flow field are very small and not

significant since Z_{st} is not varied significantly. Thus, flame structure effects are more isolated. Looking again at Eq. 2, it is observed that increasing the flame temperature, while holding Z_{st} constant (as was done in flames B and C), results in an increase in the C/O ratio at the location of precursor decomposition, $T = T_d$. The effect of increasing flame temperature is to push the precursor decomposition and particle formation zone into a region with a higher fuel concentration and a lower concentration of oxygen-containing products, resulting in a less oxidizing environment in the particle formation region. The reduction in the oxidation state with increased flame temperature observed experimentally is consistent with this description.

The effect of fuel composition is observed by considering flames C and E. These two flames differ only by the fuel composition; methane was used in flame C and ethylene in flame E. The adiabatic flame temperature, Z_{st} , and the fuel and oxidizer flow rates, were all held constant. Although there is some uncertainty in the use of the calculated flame temperature, it should be recalled that all the flames were non-luminous and radiation losses were similar in all cases. The overall iron oxidation state of sample E was much lower than that of sample C, and contained a significant fraction of α -Fe metal, indicating that the particles in flame E were formed in a less oxidizing environment. This trend is also predicted by Eq. 2 and can be observed by examining the term $m/(m+n/4)$. Thus, the switch from methane to ethylene increases the local C/O ratio by a factor of 4/3.

Other factors relating to gas composition may also be contributing to the preference for reduced Fe in the ethylene flame, compared to the methane flame. For example, acetylene is a major product of ethylene decomposition. In studies utilizing iron-containing particles as catalysts for carbon nanotube synthesis in acetylene atmospheres, it has been shown that iron oxide is reduced during the nanotube growth process (Nishimura *et al.* 2004; Sato *et al.* 2006). In addition, a greater concentration of H_2 resulting from ethylene pyrolysis could result in the reduction of iron oxide via the following reactions (Lin *et al.* 2003).



More study which includes modeling of detailed flame chemistry is needed before any hard conclusions can be reached regarding fuel composition effects on oxidation state. Nonetheless, the choice of fuel appears to be an important consideration for the synthesis of these particles.

5. Conclusions

A gas-phase, laminar diffusion flame process for the synthesis of reduced iron oxide nanoparticles has been demonstrated. The method takes advantage of the unique flame environment that can be achieved through the utilization of the inverse flame geometry and oxygen-enhanced combustion. Nanoparticles exhibiting superparamagnetic behavior composed largely of Fe_3O_4 were synthesized, as were composite particles containing α -Fe. The effects of flame temperature, stoichiometric mixture fraction, and fuel choice on the oxidation state, particle size, and magnetic properties of iron oxide particles were examined. The crystallite size, Fe(II) fraction, and saturation magnetization were all found to increase with flame temperature. These results offer the intriguing possibility of producing magnetite and other reduced transition metal oxides that are not currently synthesized in bulk using gas-phase flame synthesis. In addition to the obvious applications in nanotechnology, such particles may also be used in new remediation technologies for environmental purposes.

Acknowledgments

This publication was made possible by grant number 5 P42 ES004699 from the National Institute of Environmental Health Sciences (NIEHS), NIH and the contents are solely the responsibility of the authors and do not necessarily represent the official views of the NIEHS, NIH.

References

- Cabanas MV, Valletregi M, Labeau M, Gonzalezcalbet JM. Spherical iron-oxide particles synthesized by an aerosol technique. *J. Mater. Res* 1993;8:2694–2701.
- Dobbins RA, Megaridis CM. Morphology of Flame-Generated Soot As Determined by Thermophoretic Sampling. *Langmuir* 1987;3:254–259.
- Du J, Axelbaum RL. The effect of flame structure on soot-particle inception in diffusion flames. *Combust. Flame* 1995;100:367–375.
- du Trémolet de Lacheisserie, E.; Gignoux, D.; Schlenker, M. *Magnetism: Materials and Applications*. Springer; 2005.
- Gonzalez D, Nasibulin AG, Jiang H, Queipo P, Kauppinen EI. Electro spraying of ferritin solutions for the production of monodisperse iron oxide nanoparticles. *Chem. Eng. Commun* 2007;194:901–912.
- Grass RN, Stark WJ. Flame spray synthesis under a non-oxidizing atmosphere: Preparation of metallic bismuth nanoparticles and nanocrystalline bulk bismuth metal. *Journal of Nanoparticle Research* 2006a;8:729–736.
- Grass RN, Stark WJ. Gas phase synthesis of fcc-cobalt nanoparticles. *Journal of Materials Chemistry* 2006b;16:1825–1830.
- Grimm S, Schultz M, Barth S, Muller R. Flame pyrolysis - A preparation route for ultrafine pure gamma-Fe₂O₃ powders and the control of their particle size and properties. *J. Mater. Sci* 1997;32:1083–1092.
- Guo B, Kennedy IM. Gas-phase flame synthesis and characterization of iron oxide nanoparticles for use in a health effects study. *Aerosol Sci. Technol* 2007;41:944–951.
- Hergt R, Andra W, d'Ambly CG, Hilger I, Kaiser WA, Richter U, Schmidt HG. Physical limits of hyperthermia using magnetite fine particles. *IEEE Trans. Magn* 1998;34:3745–3754.
- Hofmeister H, Huisken F, Kohn B, Alexandrescu R, Cojocaru S, Crunteanu A, Morjan I, Diamandescu L. Filamentary iron nanostructures from laser-induced pyrolysis of iron pentacarbonyl and ethylene mixtures. *Appl. Phys. A* 2001;72:7–11.
- Janzen C, Roth P. Formation and characteristics of Fe₂O₃ nano-particles in doped low pressure H₂/O₂/Ar flames. *Combust. Flame* 2001;125:1150–1161.
- Kumar P, Biswas P. Analytical expressions of the collision frequency function for aggregation of magnetic particles. *J. Aerosol Sci* 2005;36:455–469.
- Kumfer, BM. Dissertation. St. Louis, MO.: Washington University; 2005. Design of diffusion flame structure for reduced soot using oxygen-enriched combustion.
- Kumfer BM, Skeen SA, Axelbaum RL. Soot inception limits in laminar diffusion flames with application to oxy-fuel combustion. *Combust. Flame* 2008;154:546–556.
- Kumfer BM, Skeen SA, Chen R, Axelbaum RL. Measurement and analysis of soot inception limits of oxygen-enriched coflow flames. *Combust. Flame* 2006;147:233–242.
- Langlet M, Labeau M, Bochu B, Joubert JC. Preparation of thin-films in the system gamma-Fe₂O₃-Fe₃O₄ for recording media by spray pyrolysis of organometallic solutions using an ultrasonic pump. *IEEE Trans. Magn* 1986;22:151–156.
- Li D, Teoh WY, Selomulya C, Woodward RC, Munroe P, Amal R. Insight into microstructural and magnetic properties of flame-made -Fe₂O₃ nanoparticles. *Journal of Materials Chemistry* 2007;17:4876–4884.
- Lin H-Y, Chen Y-W, Li C. The mechanism of reduction of iron oxide by hydrogen. *Thermochim. Acta* 2003;400:61–67.
- Makel DB, Kennedy IM. Soot Formation in Laminar Inverse Diffusion Flames. *Combust. Sci. Tech* 1994;97:303–314.
- Makela JM, Keskinen H, Forsblom T, Keskinen J. Generation of metal and metal oxide nanoparticles by liquid flame spray process. *J. Mater. Sci* 2004;39:2783–2788.

- McBride BJ, Gordon S. Computer program for calculation of complex chemical equilibrium compositions and applications, National Aeronautics and Space Administration, NASA RP-1311-P2. 1996:178.
- Miyake S, Kinomura N, Suzuki T, Suwa T. Fabrication of spherical magnetite particles by the flame fusion method. *J. Mater. Sci* 1999;34:2921–2928.
- Nishimura K, Okazaki N, Pan L, Nakayama Y. In Situ Study of Iron Catalysts for Carbon Nanotube Growth Using X-Ray Diffraction Analysis. *Jap. J. Appl. Phys* 2004;43:L471.
- O'Day PA, Rivera N Jr, Root R, Carroll SA. X-ray absorption spectroscopic study of Fe reference compounds for the analysis of natural sediments. *American Mineralogist* 2004;89:572–585.
- Pratsinis SE. Flame aerosol synthesis of ceramic powders. *Prog. Energy Combust. Sci* 1998;24:197–219.
- Pratsinis SE, Zhu W, Vemury S. The role of gas mixing in flame synthesis of titania powders. *Powder Technol* 1996;86:87–93.
- Sato H, Hori Y, Hata K, Seko K, Nakahara H, Saito Y. Effect of catalyst oxidation on the growth of carbon nanotubes by thermal chemical vapor deposition. *J. Appl. Phys* 2006;100:104321.
- Schleicher B, Tapper U, Kauppinen EI, Martin M, Roschier L, Paalanen M, Wernsdorfer W, Benoit A. Magnetization reversal measurements of size-selected iron oxide particles produced via an aerosol route. *Appl. Organomet. Chem* 1998;12:315–320.
- Sidebotham GW, Glassman I. Effect of oxygen addition to a near-sooting ethene inverse diffusion flame. *Combust. Sci. Tech* 1992;81:207–219.
- Smirnov VN. Thermal dissociation and bond energies of iron carbonyls Fe(CO)(N) (N=1–5). *Kinet. Catal* 1993;34:523–530.
- Stark WJ, Pratsinis SE. Aerosol flame reactors for manufacture of nanoparticles. *Powder Technol* 2002;126:103–108.
- Sunderland PB, Urban DL, Stocker DP, Chao B-H, Axelbaum RL. Sooting limits of microgravity spherical diffusion flames in oxygen-enriched air and diluted fuel. *Combust. Sci. Tech* 2004;176:2143–2164.
- Taguchi T, Shinoda K, Tohji K. *Phys. Scr. T* 2005;T115:1017–1018.
- Tang ZX, Nafis S, Sorensen CM, Hadjipanayis GC, Klabunde KJ. Magnetic properties of aerosol synthesized iron oxide particles. *J. Magn. Magn. Mater* 1989;80:285–289.
- Unrau CJ, Axelbaum RL, Biswas P, Fraundorf P. Synthesis of single-walled carbon nanotubes in oxy-fuel inverse diffusion flames with online diagnostics. *Proc. Combust. Instit* 2007;31:1865–1872.
- Urakawa T, Nakazawa T, Inoue H, Shirai T, Flock E. Preparation and Mössbauer spectroscopic characterization of ultrafine iron oxide particles. *J. Mater. Sci. Lett* 1996;15:1237–1239.
- Wooldridge MS. Gas-phase combustion synthesis of particles. *Prog. Energy Combust. Sci* 1998;24:63–87.
- Wu KT, Essenhigh RH. Comparison of normal and inverse diffusion flames of methane. *Proc. Combust. Instit* 1986;20:1925–1935.
- Zachariah MR, Aquino MI, Shull RD, Steel EB. Formation of superparamagnetic nanocomposites from vapor phase condensation in a flame. *Nanostruct. Mater* 1995;5:383–392.
- Zhu W, Pratsinis SE. Synthesis of SiO₂ and SnO₂ particles in diffusion flame reactors. *AIChE Journal* 1997;43:2657–2664.
- Zimmer AT, Biswas P. Characterization of the aerosols resulting from arc welding processes. *J. Aerosol Sci* 2001;32:993–1008.

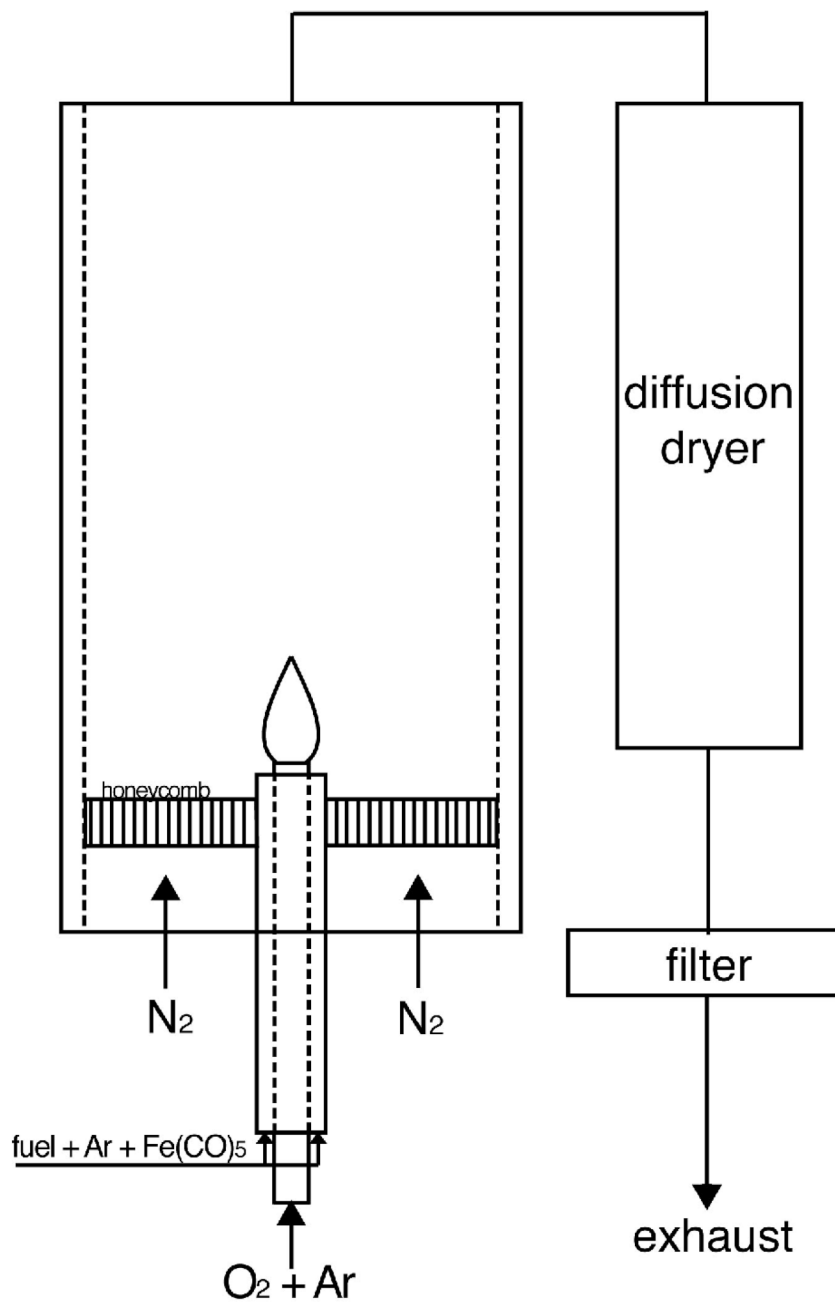


Figure 1.
Experimental setup for flame synthesis of iron oxide nanoparticles.

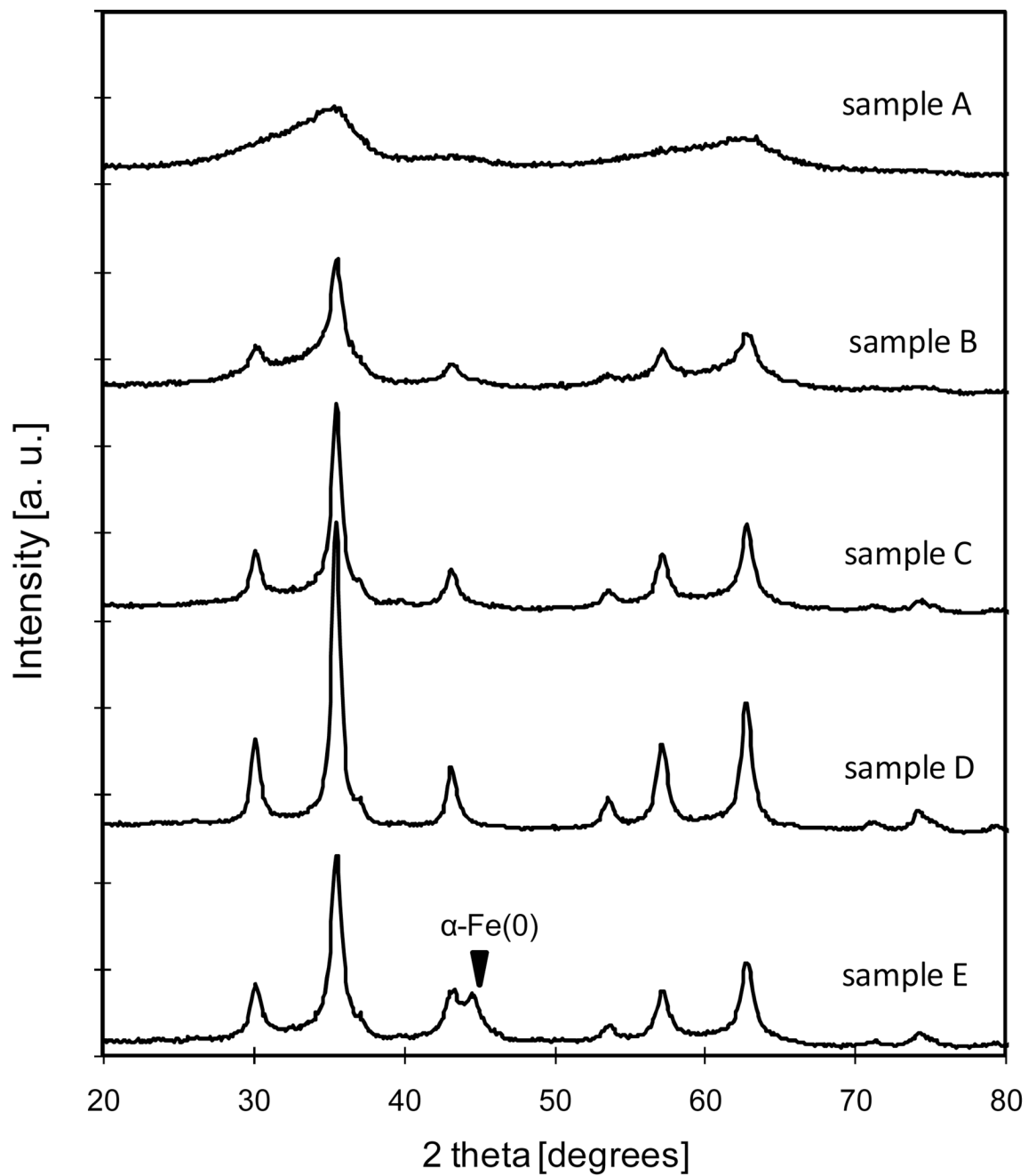


Figure 2.
Powder X-ray diffraction patterns of as-produced iron oxide nanoparticles.

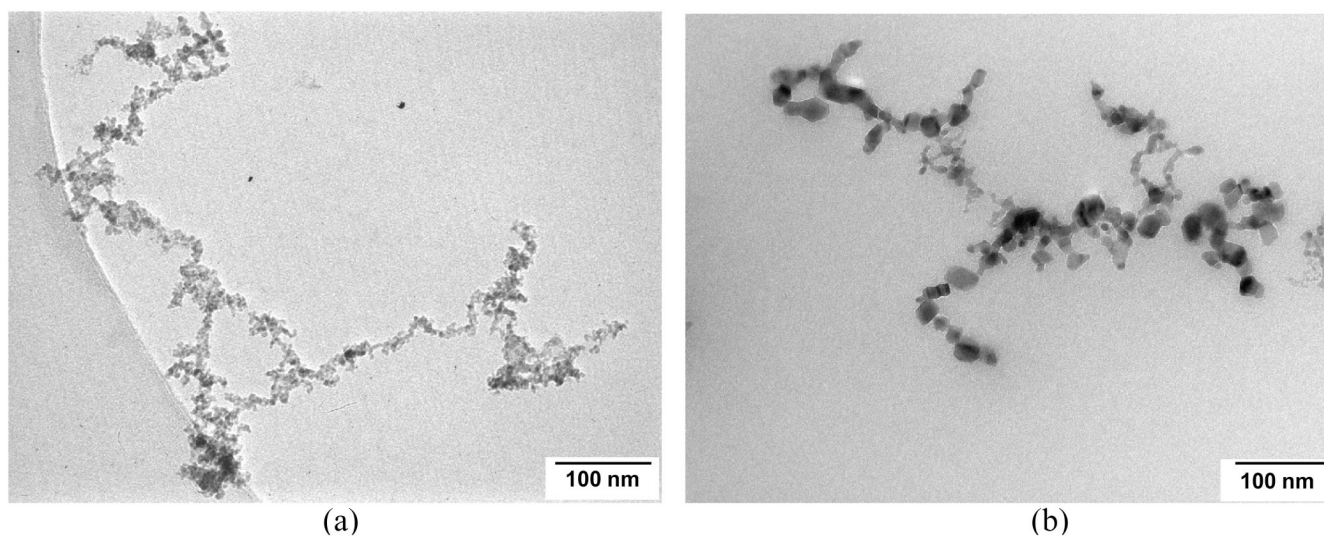


Figure 3. TEM images of iron oxide nanoparticles (a) sample A, $T_{ad} = 2150$ K, $Z_{st} = 0.35$. (b) sample D, $T_{ad} = 2650$ K, $Z_{st} = 0.79$.

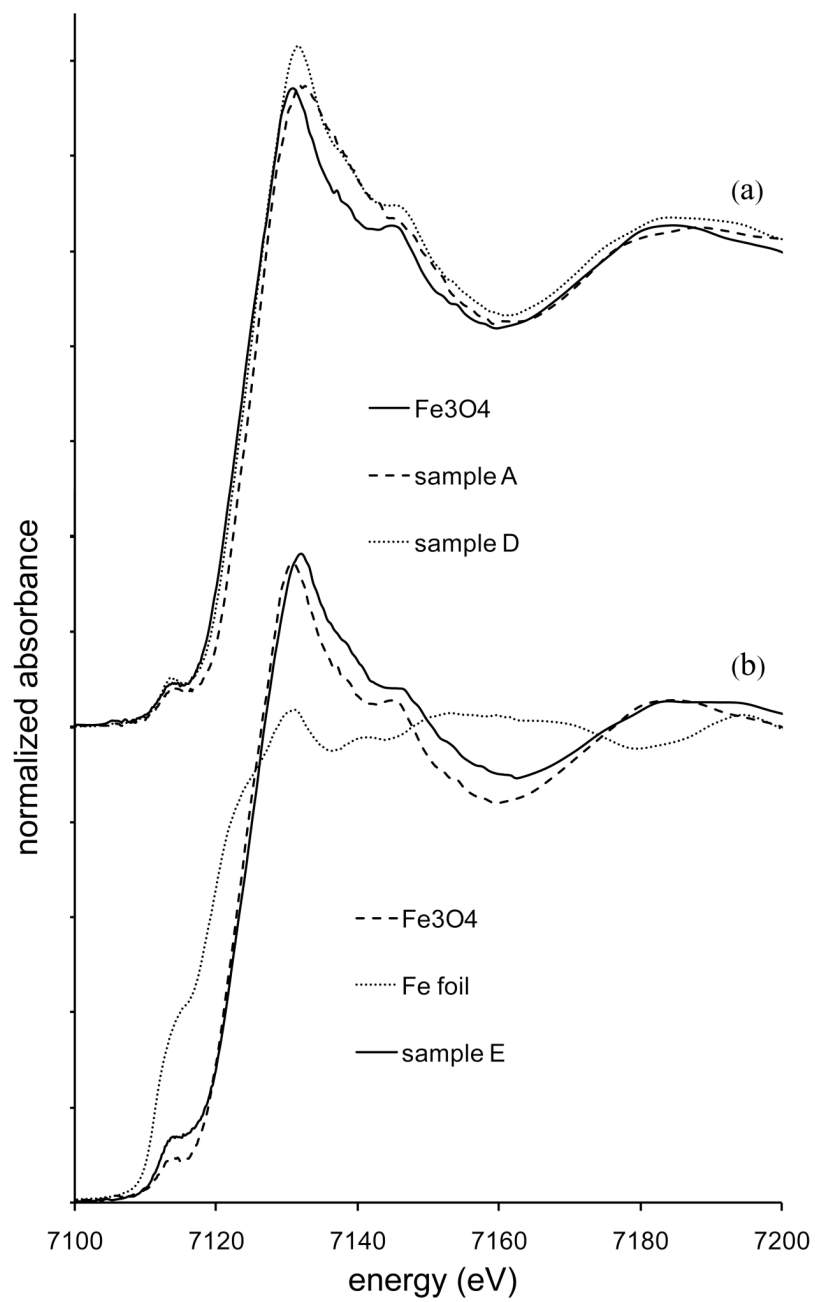


Figure 4. XANES spectra of iron oxide particle samples and Fe₃O₄ and Fe foil reference samples.

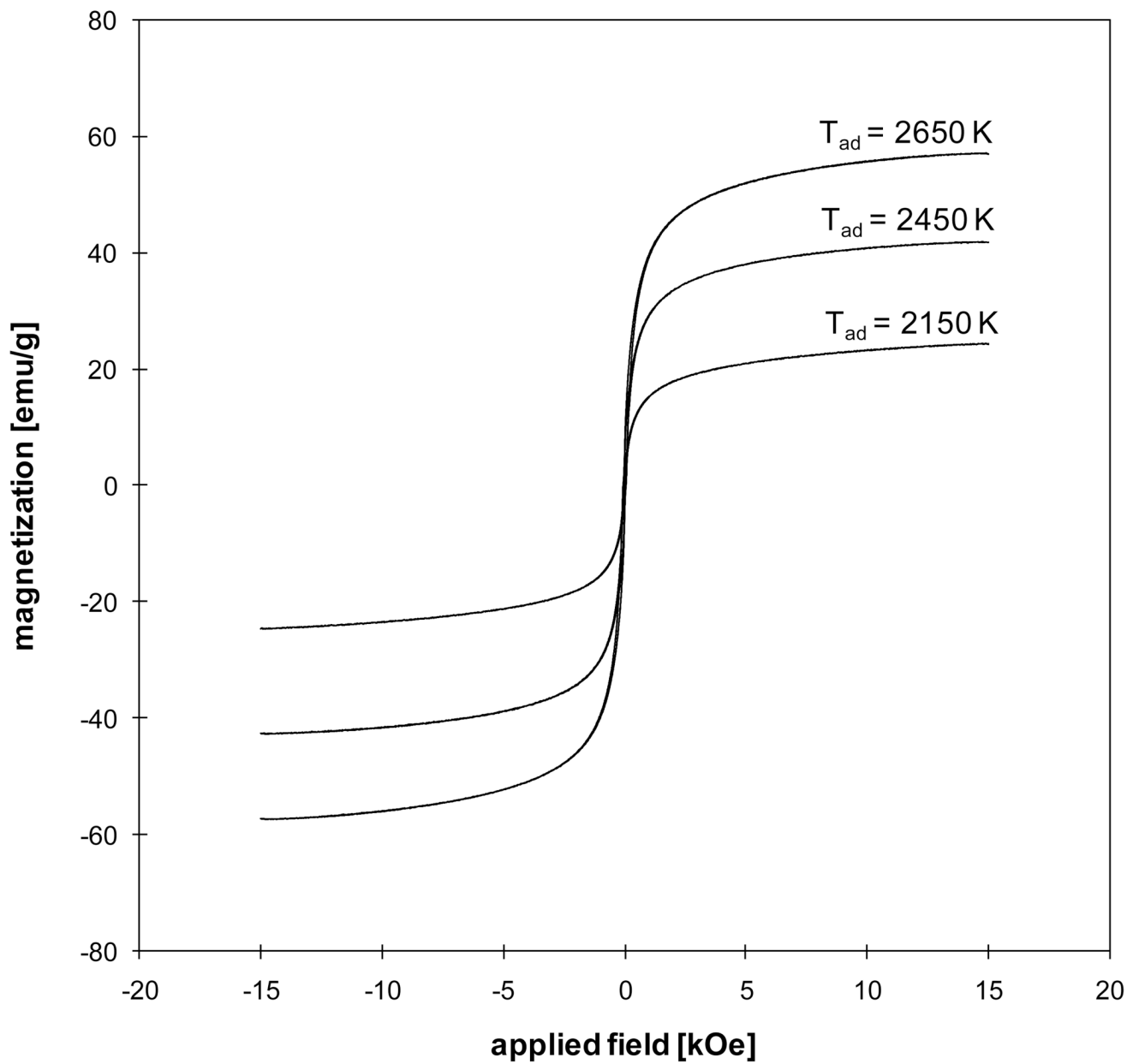


Figure 5. Hysteresis loops of iron oxide particles produced in a high- Z_{st} flame of methane.

Table 1

Summary of flame and particle properties

sample	fuel	flame properties					particle properties			
		Q_{ox} (SLPM)	X_O	X_F	Z_{st}	T_{ad} (K)	D_{cr} (nm)	M_S (emu/g)	H_c (Oe)	
A	CH ₄	0.70	0.20	0.17	0.35	2150	2.9	6.5	13	
B	CH ₄	0.17	0.75	0.07	0.85	2150	7.9	24	19	
C	CH ₄	0.19	1.0	0.10	0.85	2450	11	42	30	
D	CH ₄	0.25	1.0	0.15	0.79	2650	12	57	60	
E	C ₂ H ₄	0.15	0.86	0.06	0.85	2450	n/a	60	76	

Q_{ox} = flow rate of the oxidizer stream. X_O = mole fraction of oxygen in oxidizer stream. X_F = mole fraction of fuel in fuel stream. Z_{st} = stoichiometric mixture fraction. T_{ad} = adiabatic flame temperature. D_{cr} = XRD crystallite diameter. M_S = saturation magnetization. H_c = coercivity